

Anodization growth of self-organized ZrO₂ nanotubes on zircaloy-4. Evaluation of the photocatalytic activity

Patricia María Perillo¹, Daniel Fabián Rodríguez²

¹Comisión Nacional de Energía Atómica, Centro Atómico Constituyentes, Depto. Micro y Nanotecnología, Av. Gral. Paz 1499 (1650) Bs. As. Argentina
e-mail: perillo@cnea.gov.ar

²Comisión Nacional de Energía Atómica, Centro Atómico Constituyentes, Depto. Micro y Nanotecnología, Av. Gral. Paz 1499 (1650) Bs. As., Argentina
e-mail: daniel.cnea@gmail.com

RESUMEN

Nanotubos de ZrO₂ se prepararon a través de oxidación anódica en un electrolito orgánico de glicerina conteniendo fluoruro de amonio. La morfología de estas matrices de nanotubos puede ser controlada cambiando los parámetros de preparación, tales como la tensión aplicada, la concentración de iones fluoruro y el tiempo de anodización. Mientras que la tensión de la oxidación es el factor principal que controla el diámetro de los nanotubos, la longitud de los mismos depende principalmente del tiempo de oxidación, y el tipo de cristal está estrechamente relacionado con la temperatura de recocido. También se estudió el desempeño fotocatalítico. La actividad fotocatalítica de las muestras se calculó por la degradación de un colorante patrón, bajo iluminación de luz halógena.

Palabras clave: ZrO₂, zircaloy-4, anodización, fotocatalisis.

ABSTRACT

ZrO₂ nanotube arrays were prepared through anodic oxidation in glycerol organic electrolyte containing ammonium fluoride. The morphology of these nanotube arrays can be controlled by changing the preparation parameters such as applied voltage, fluoride ion concentration and time of anodization. While the oxidation voltage is the main factor that controls the diameter of nanotubes, the length of nanotubes is mainly depending on the oxidation time, and the crystal type is closely related to the annealing temperature. We also studied their photocatalytic performance. The photocatalytic activity of samples was calculated by the degradation of a model dye, under halogen light illumination.

Keywords: ZrO₂, nanotubes, zircaloy-4, anodization, photocatalytic.

1. INTRODUCTION

Zirconia has been widely studied because of its attractive technological properties, including high thermal and chemical stability, good mechanical strength and wear resistance, excellent dielectric properties (as oxide of a “valve metal”) and good ion-exchange properties.

Due to their prominent physical and chemical properties, zirconia (ZrO₂) ceramic materials have been widely used in modern engineering and industry fields, such as chemical sensors [1,2], fuel cells [3], thermal barrier coatings [4], refractory materials [5], catalysts [6-8], biomedical applications [9-11].

One of the main uses of zirconium alloys is in nuclear technology, as cladding of fuel rods in nuclear reactors, especially water reactors because of their low capture cross-section for thermal neutrons, high hardness, ductility and good mechanical and corrosion properties. Pods of fuel elements and many of the structural components operating in nuclear power reactors are manufactured with Zircaloy-4 (Zry-4), alloy base zircon reference for the nuclear industry [12,13].

The nanotubes formed on zirconium have close similarities with those produced on titanium [14,15]; similar electrolytes can be used to grow nanotubes on the two metals. The nanotubes on both metals have

dimensions related to the growth conditions, with the tube diameter increasing with increase of the anodizing applied potential [16-18].

In this study, the effect of some experimental parameters as concentration of ammonium fluoride (NH_4F) and voltage on ZrO_2 nanotubes morphology was investigated. We also studied their photocatalytic performance by the degradation of methyl red (MR) under halogen light illumination.

2. EXPERIMENTAL DETAILS

3. 2.1. MATERIALS

The material used is Zry-4 which conforms to the ASTM B-352 standard Zry-4 nuclear grade. Table 1 shows the chemical composition of Zry-4 nuclear grade. This is a completely recrystallized material with a grain of 20 microns in diameter.

Table 1: Chemical composition of Zry-4 nuclear grade used for anodization.

Alloys (%)									
Sn		Fe			Cr			O	
1.49		0.20			0.11			0.14	
Impurities (ppm)									
Ni	Hf	Al	Co	Cu	Mn	Mo	Ti	U	W
49	99	39	18	30	36	8	3	1.5	25

The glycerol (anhydrous > 99%), ammonium fluoride (NH_4F) 40%, hydrofluoric acid (HF) \geq 40%, and nitric acid (HNO_3) 65-68% were of analytical grade and used as received without further purification.

2.2. Synthesis

The anodization was conducted in a two electrode electrochemical cell with a platinum foil as cathode and Zry-4 foil as anode at a constant potential. All anodization experiments were carried out at room temperature and the solutions were stirred using a magnetic stirrer. Zry-4 specimens were cut into (15 mm \times 10 mm \times 0.4 mm) samples. Prior to the experiments, the samples were pickled in a solution of 10 vol.% hydrofluoric acid, 45 vol.% nitric acid and 45 vol.% distilled water for 1 min to remove inorganic contamination from the fabrication process, afterwards rinsed with deionized water (DI) and finally dried in a nitrogen stream.

The growth of the nanotube arrays has been obtained using a glycerol solution at two concentrations of ammonium fluoride [19]. The back side and edges of the samples were masked with an epoxy lacquer leaving an area of 1 cm^2 in contact with the solution. The electrolyte was maintained at room temperature.

Anodizing was carried out at 20, 40, 60, 80 and 100 V, applying a ramp during 3 min from 0 to the desire voltage and finally holding the constant voltage from 30 min to 3 h using a 2612A Keithley system sourcemeter.

The distance between the two electrodes was kept at 2 cm in all the experiments. Then the nanotube films were annealed in air at different temperatures for 2 hours.

2.3 Characterization

The samples were characterized by scanning electron microscopy (SEM) and X-ray diffraction (XRD). Scanning electron microscopes (Zeiss Supra40 Gemini and Fei model Quanta 200) were employed for the morphological characterization of the ZrO_2 nanotubes samples and analysis of pictures were performed by ImageJ.

X-ray diffraction (XRD) patterns were recorded at room temperature with $\text{Cu K}\alpha$ radiation of 0.15418 nm in a diffractometer (PANalytical model Empyrean) having theta-theta configuration and a graphite secondary-beam monochromator, using a generator voltage of 40 kV and current of 40 mA. The data were collected for scattering angles (2θ) ranging from 20° to 65° with a step of 0.026° for 2 s per point.

2.4. Photocatalytic activity

The photocatalytic experiments were carried out by periodically measuring photodegradation of MR aqueous solution under visible light illumination of the ZrO₂ samples immersed in the dye solution. For this, a MR solution of 7 mg/L was poured into a glass beaker. The volume of solution used was 15 ml. The dye solution without samples was used as reference. The solution in the beaker was continuously stirred at 300 rpm. The surface area of the nanotubes tested was 1 cm². A 500 W halogen lamp was used as the visible light irradiation (the emission maximum at $\lambda_{\text{max}} = 560$ nm and less than 0.3% the emitted fall in the UVA). The reflector lamp has a parabolic geometry in order to generate a parallel beam of light. The horizontal distance between ZrO₂ nanotubes and light source was 30 cm. Prior to the illumination the solution was kept for 30 min in the dark to achieve the equilibrium of adsorption and desorption. Afterwards the samples were irradiated. A cooling fan at the top and sides of the lamp removed the lamp heat.

The absorbance of MR solution was measured by a UV-Vis spectrophotometer (UV-1800, Shimadzu, Japan) and the MR concentrations were used to determine the pseudo-first order reaction rate constant (k , min⁻¹) and degradation efficiency (%) by using the following equations [20,21]:

$$\ln C_0/C = \ln A_0/A = kt \quad (1)$$

$$\text{Degradation efficiency (\%)} = C - C_0 / C_0 \times 100 = A - A_0 / A_0 \times 100 \quad (2)$$

Where C is the concentration of MR after t min. of reaction and C_0 is the initial concentration. The parameter A_0 and A are the absorbance of the MR solution in the 432 nm wavelength at initial and any time respectively. The k value was calculated from slope of the plot between $\ln(A_0/A)$ and time (t).

3. RESULTS

3.1. Influence of anodization voltage

In order to find the suitable conditions for the synthesis of ZrO₂ nanotube arrays, we studied the effect of applied voltage while keeping the content of NH₄F constant. Fig.1 shows the SEM images of the prepared samples in glycerol containing 1.2 wt.% NH₄F after anodization at applied voltages of 40, 60, 80 and 100 V. With the increasing of the applied voltage to 100 V (fig 1d) the surface has an irregular and disordered appearance with bundled and collapsed nanotubes.

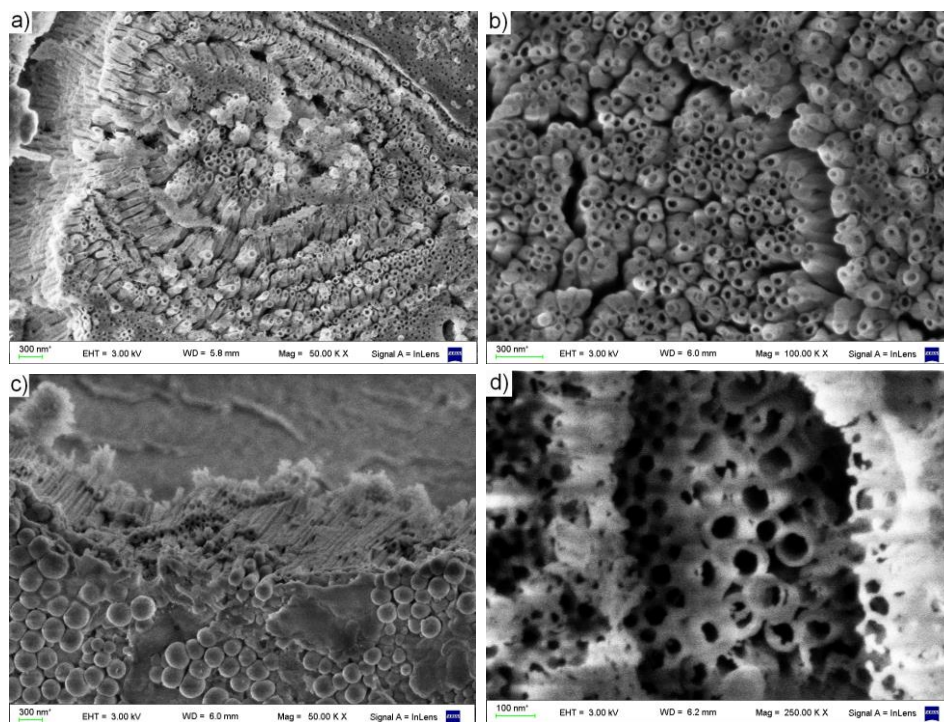


Figure 1: SEM images of ZrO₂ nanotubes prepared at different voltages (a) 40 V (top view); (b) 60 V (top view); (c) 80 V (bottom view); (d) 100 V (top view).

Fig. 2 is a side view of nanotubes prepared at 60 V. The length of nanotubes reached up to 3.6 μm after 3 h of anodization.

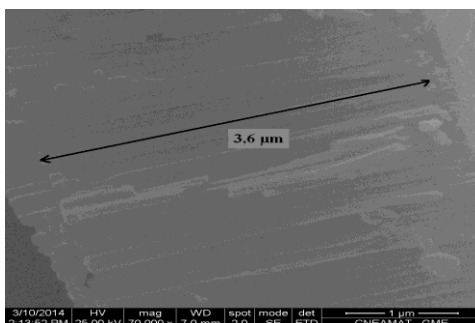


Figure 2: Side view of ZrO_2 nanotubes obtained at 60 V.

It is well known that the voltage is an important parameter to control the tube diameter and wall thickness [22,23]. The higher the applied voltage, the stronger the electric field applied on the substrates [24, 25]. As shown in Fig. 3 an increase of applied voltage produced even larger nanotubes with diameters from 45 nm to 70 nm for 0.6 wt.% NH_4F and 85 to 260 nm for 1.2 wt.% NH_4F . The wall thickness is almost the same with increasing of applied voltage from 40 to 100 V.

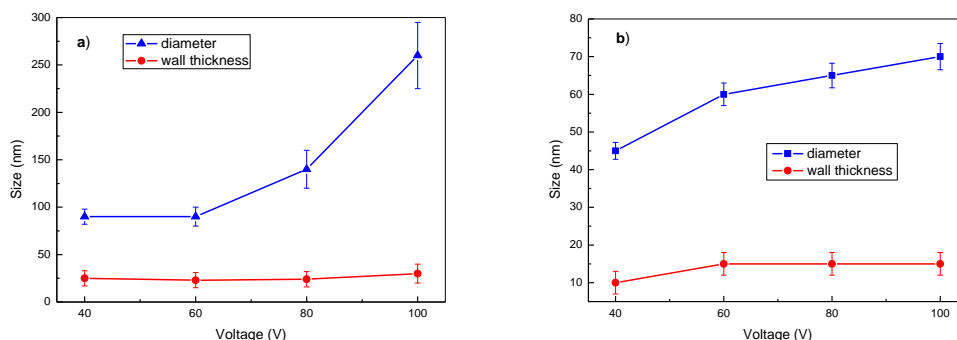
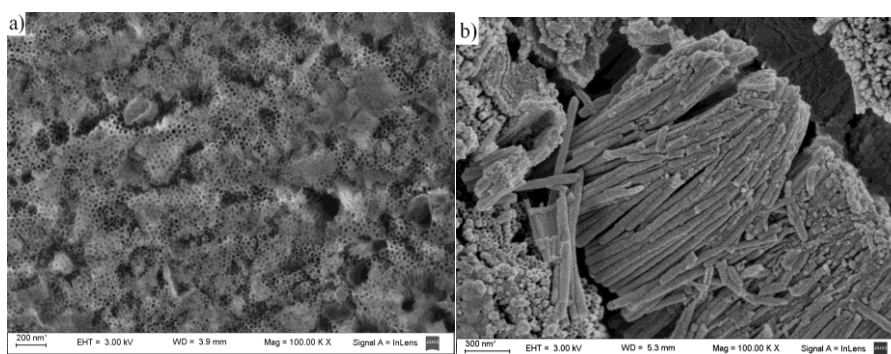


Figure 3: Diameter average and wall thickness of nanotubes as a function of applied voltage containing a) 1.2 wt.% NH_4F b) 0.6 wt.% NH_4F .

As shown in Fig.1 it was found that the optimum voltage for the formation of nanotubular ZrO_2 structures was 60 V with 1.2 wt% NH_4F solution and 3 h anodization time.

3.2. Effect of NH_4F concentration

In a second series of experiments, concentration of NH_4F was changed from 0.6 to 1.2 wt.%, and variations of diameter size of nanotubes were studied. Fig. 4 shows the morphology of ZrO_2 nanotubes obtained from these experiments. By increasing the NH_4F content, the diameter of nanotubes increases from 60 to 85 nm at 60 V applied voltage (fig 4 a,c). Fig 4b,d correspond to a side view of the same nanotubes.



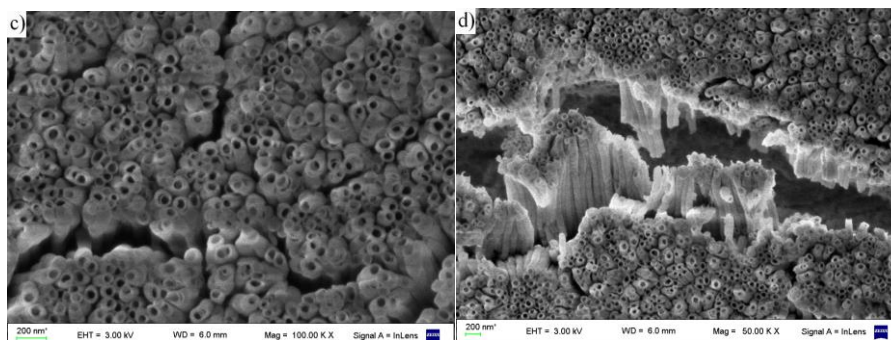


Figure 4: SEM images of ZrO₂ nanotubes prepared with a constant anodizing voltage of 60 V using (a) 0.6 wt.% NH₄F (top view); (b) 0.6 wt.% NH₄F (side view); (c) 1.2 wt% NH₄F (top view); (d) 1.2 wt% NH₄F (side view).

The average wall thickness of the resulting nanotube arrays seems to roughly remain the same with an average wall thickness of 15 nm (0.6wt.% NH₄F) and 20 nm (1.2 wt% NH₄F, respectively (Fig 3 a,b).

3.3. Current/time transient at constant voltage

Fig. 6 shows the current transients (I–t curve) recorded during the anodization process. In the first stages of the anodization process, the current increases rapidly owing to the increases of the voltage applied. Then the current drops drastically owing to the formation of a thin oxide layer formed on the surface of the Zry-4 sheet.

As a result fine pits or pores are formed at the surface Fig 6 (a). Under sufficient applied voltage magnitude, field-assisted oxidation occurs at the ZrO₂/Zr interface, where the oxygen ions (O₂[−]) are transported from the solution to the oxide layer.

Fig 6 (b) corresponds to the point where the nanotubes structure is formed. Fig 6 (c) refers to the point where the layer is more uniform and regular.

Afterwards, the current density decays and then reaches the stable-state, which is a signal that the formation of pore reaches equilibrium with the dissolution. Fig 6 (d). After anodization of 3 h, a nanotubular structure is formed. In summary, the ZrO₂ nanotube formation in F[−] containing electrolytes is the result of a competition between an electrochemical oxide formation and chemical dissolution of oxide by fluoride ions [26,27].

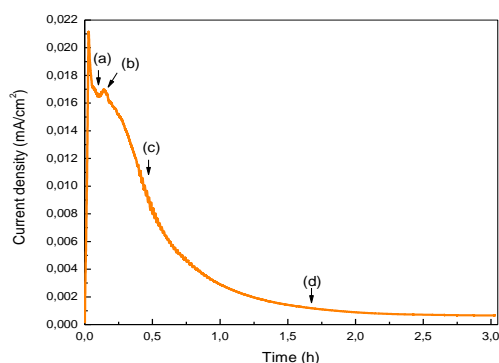


Figure 6: Curve of current density vs time during anodization

The reactions can be depicted as follows [28]:

i) Oxide growth at the surface of the metal due to the interaction of metal with O^{−2} of OH[−] ions.



ii) In the presence of fluoride ions, Zr^{4+} ions arriving at the oxide/solution interface are resolved to ZrF_6^{2-}



3.4. XRD analysis

The as-prepared samples possessed amorphous structures, while both monoclinic and tetragonal phases were found after annealing at a temperature between 400°C and 650 °C. In the case of zirconia, there are three familiar phases namely monoclinic phase, tetragonal phase, and cubic phases.

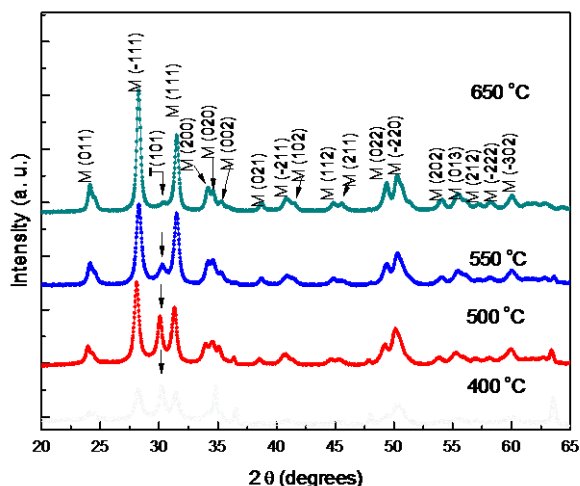


Figure 7: XRD patterns of ZrO_2 annealed at different temperatures.

At 400°C, the diffraction peaks are indexed as the tetragonal phase (JCPDS Card No. 42-1164) (011), (-111), (-220), (111)) at $2\theta = 30.15^\circ$ while peaks of monoclinic zirconia (JCPDS Card No. 37-1484) (101), (110) at $2\theta = 28.22$, and $2\theta = 31.5$ also appear. At 650°C, a main peak for the monoclinic phase increased, while a peak of tetragonal zirconia decreased. Monoclinic (M) and tetragonal (T) zirconia coexisted when annealed between 400 °C and 650 °C and the content of monoclinic phase increases gradually with increasing temperature of calcination. When the annealing temperature increases, the tetragonal phase decreases and disappears over 650°C [29].

3.5. Photocatalytic activity

The photoactivity of the catalysis of ZrO_2 nanotubes prepared at anodizing voltage of 60 V using 1.2 wt.% NH_4F was evaluated by the heterogeneous degradation of MR aqueous solution [30] under visible light irradiation, and the results were shown in fig. 8 a. When the sample was irradiated for 120 min the degradation percentage of MR reached 25 %. The blank (absence of photocatalys) experiment was also carried out and less than 1% of MR removal was observed for 120 min irradiation.

Fig 8 b shows the kinetic behaviour of photocatalytic degradation of MR by ZrO_2 nanotubes. The plot of $\ln(C_0/C)$ vs. Irradiation time exhibits a straight line and the slope is equal to the pseudo first order rate constant k . The observed linear relationship indicates that the MR decomposition follows a first order kinetic reaction [31]. The estimated value of the pseudo first order rate constant was 0.0026 min^{-1} .

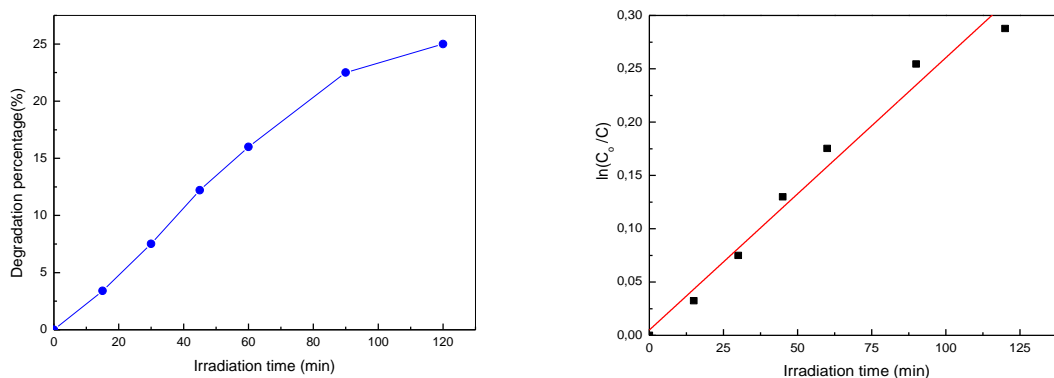


Figure 8: Photocatalytic activity of ZrO₂ nanotubes a) degradation percentage b) pseudo first order kinetic curve

The photocatalytic mechanism for degradation of organic pollutants can be explained [32]. Under visible light illumination, electrons (e⁻) migrate from the valence band to the conduction band. Meanwhile, holes (h⁺) will be left at the valence band. The holes can oxidize donor molecules (D) whereas the conduction band electrons can reduce appropriate electron acceptor molecules (A). A characteristic feature of semiconducting metal oxides is the strong oxidation power of their holes h⁺. They can react in an one-electron oxidation step with water to produce the highly reactive hydroxyl radical (OH[•]). Both the holes and the hydroxyl radicals are very powerful oxidants, which can be used to oxidize most organic contaminants.

4. 4. CONCLUSIONS

Zirconia nanotube arrays were prepared using direct anodization of Zry-4 in glycerol containing NH₄F. The diameter of the nanotubes was about 85 nm with a length of up to 3.6 μm when anodization took place at 60 V for 3 h. Monoclinic and tetragonal zirconia coexisted when annealed at 400 °C and 650 °C. The photocatalytic ability of the nanotubes was assessed. The top degradation rate reached 25% after 120 minutes. It appears that MR could be degraded under visible illumination in the presence of ZrO₂ nanotubes.

In the present work it is indicated that Zry-4 is propitious for the preparation of ZrO₂ nanotubes. Further studies on growth control of ZrO₂ nanotubes are necessary for tailoring the oxide layer in some specific applications such as critical heat flux in nuclear power plants.

5. BIBLIOGRAPHY

- [1] SHIMIZU, K., CHINZEI, I., NISHIYAMA, H., et al., "Hydrogen sensor based on WO₃ subnano-clusters and Pt co-loaded on ZrO₂", *Sensors and Actuators B*, v.134, n. 2, pp. 618–624, sept. 2008.
- [2] PARK, H.J., CHOI, G.M., "Oxygen permeation characteristics of zirconia with surface modification", *Solid State Ionics*, n.177, pp. 2261–2267, oct. 2006.
- [3] LAUKAITIS, G., DUDONIS, J., MILCIUS, D. "YSZ thin films deposited by e-beam technique", *Thin Solid Films*, n.515, v.2, pp. 678-682, oct. 2006.
- [4] KITAZAWA, R., KAKISAWA, H., KAGAWA, Y. "Anisotropic TGO morphology and stress distribution in EB-PVD Y₂O₃-ZrO₂ thermal barrier coating after in-phase thermo-mechanical test", *Surface and Coating Technology*, v.238, pp. 68-74, jan. 2014.
- [5] VÁZQUEZ CARBAJAL, G.I., RODRÍGUEZ GALICIA, J.L., RENDÓN ÁNGELES, J.C., et al, *Ceramics International*, v.38, n. 2, pp. 1617-162, mar. 2012.
- [6] ATRIBAK, I., SUCH-BASANIEZ, I., BUENO-LOPEZ, A., et al, "Comparison of the catalytic activity of MO₂ (M = Ti, Zr, Ce) for soot oxidation under NO_x/O₂", *Journal of Catalysis*, v. 250, n.1, pp. 75-84, aug. 2007.
- [7] MAHMOUD, H. R. "Highly dispersed Cr₂O₃-ZrO₂ binary oxide nanomaterials as novel catalysts for ethanol conversion", *Journal of Molecular Catalysis A*, v. 392, pp 216-222, oct. 2014.
- [8] YAMAMOTO, N., SATO, S., TAKAHASHI, R., et al, "Synthesis of 3-buten-1-ol from 1,4-butanediol over ZrO₂ catalyst", *Journal of Molecular Catalysis A*, v.243 pp. 52–59, jan. 2006.
- [9] PARK, N.R., SONG, CH.G., SHON, I.J. "Fast low-temperature consolidation of a nanostructured 2Ti-ZrO₂ composite for biomedical applications", *Ceramics International*, v. 40, n. 4, pp. 6311–6317, may 2014.

- [10] YEN, S.K, GUO, M.J, ZAN, H.Z. “Characterization of electrolytic ZrO₂ coating on Co–Cr–Mo implant alloys of hip prosthesis”, *Biomaterials* , v. 22, n.2, pp.125–133, jan. 2001.
- [11] LIU, X., HUANG, A., DING, C., et al, “Bioactivity and cytocompatibility of zirconia (ZrO₂) films fabricated by cathodic arc deposition “, *Biomaterials* , n. 27, pp. 3904–3911, july 2006.
- [12] GRIFFITHS, M., GILBERT, R.W., FIDLERIS, V. *Zirconium in the nuclear industry: Eighth International Symposium, ASTM STP 1023*, American Society for Testing Materials, Philadelphia, 658- 677, 1989.
- [13] LEE, C., KIM, H., AHN, H.S., et al, “Micro/nanostructure evolution of zircaloy surface using anodization technique: Application to nuclear fuel cladding modification”, *Applied Surface Science*, v. 258 , n.22, pp. 8724-8731, sept. 2012.
- [14] VALOTA, A., LECLERE, D.J., SKELDON, P., et al, “Influence of water content on nanotubular anodic titania formed in fluoride/glycerol electrolytes”, *Electrochimica Acta*, v. 54, pp. 4321- 4327, july 2009.
- [15] ZHAO, J., WANG, X., XU, R., et al., “Fabrication of high aspect ratio zirconia nanotube arrays by anodization of zirconium foils”, *Materials Letters*, v. 62, pp. 4428-4430, nov. 2008.
- [16] GONG, D., GRIMES, C.A., VARGHESE, O.K., et al, “Titanium oxide nanotube arrays prepared by anodic oxidation”, *Journal of Materials Research*, v. 16, pp. 3331-3334, jan. 2001.
- [17] GE, R., FU, W., YANG, H., et al, “Fabrication and characterization of highly-ordered titania nanotubes via electrochemical anodization”, *Materials Letters*, v. 62, pp. 2688-2691, jun. 2008.
- [18] MACAK, J. M., SCHMUKI, P. “Anodic growth of self-organized anodic TiO₂ nanotubes in viscous electrolytes”, *Electrochimica Acta*, v. 52 pp. 1258-1264, nov. 2006.
- [19] LI, Y., MA, Q., HAN, J., et al, “Controllable preparation, growth mechanism and the properties research of TiO₂ nanotube arrays”, *Applied Surface Science*, v. 297, pp 103-108, april 2014.
- [20] KONSTANTINOOU, I.K., ALBANIS, T.A. “TiO₂-assisted photocatalytic degradation of azo dyes in aqueous solution: kinetic and mechanistic investigations: a review”, *Appl. Catal. B: Environ.*, v. 19, pp 1–14, 2004.
- [21] WONGKALASIN, P., CHAVADEJ, S., SREETHAWONG, T. “Photocatalytic degradation of mixed azo dyes in aqueous wastewater using mesoporous-assembled TiO₂ nanocrystal synthesized by a modified sol–gel process”, *Colloids Surf. A: Phys.Eng. Asp.*, v. 384, pp. 519–528, 2011.
- [22] MACÁK, J.M. Growth of anodic self-organized titanium dioxide nanotube layers, Als Dissertation genehmigt von der Technischen Fakultät der Universität Erlangen-Nürnberg, Erlangen, Germany, pag.163, 2008.
- [23] GRIMES, C.A., MOR, G.K. *TiO₂ Nanotube Arrays, Synthesis, Properties, and Applications*, Springer Science, Business Media, LLC, New York, 2009.
- [24] KANECO, S., CHEN, Y., WESTERHOFF, P., et al, “Fabrication of uniform size titanium oxide nanotubes: Impact of current density and solution conditions”, *Scripta Materialia* , v.56, pp. 373-376, 2007.
- [25] MACAK, J.M., HILDEBRAND, H., MARTEN-JAHNS, U., et al. “Mechanistic aspects and growth of large diameter self-organized TiO₂ nanotubes”, *Journal of Electroanalytical Chemistry*, n.621, pp. 254-266, sept. 2008.
- [26] MACAK, J.M, TSUCHIYA, H., GHICOV, A., et al, “TiO₂ nanotubes: Self-organized electrochemical formation, properties and applications”, *Current Opinion in Solid State and Materials Science*, v.11, n.1-2, pp. 3–18, february-april 2007.
- [27] ISMAY, S., AHMAD, Z., BERENOV, A., et al, “Effect of applied voltage and fluoride ion content on the formation of zirconia nanotube arrays by anodic oxidation of zirconium”, *Corr. Sci.*, v.53 pp. 1156–1164, 2011.
- [28] HIROAKI, T., MACAK, J. M., IRINA, S., et al., “Self-organized high-aspect-ratio nanoporous zirconium oxides prepared by electrochemical anodization”, *Small*, v.1, n.7, pp. 722-725, 2005.
- [29] JIANG, W., HE, J., ZHONG, J., et al, “Preparation and photocatalytic performance of ZrO₂ nanotubes fabricated with anodization process”, *Applied Surf. Sci.*, v.307, pp.407-413, 2014.
- [30] PANG, Y. L., ABDULLAH, A. Z., “Comparative study on the process behavior and reaction kinetics in sonocatalytic degradation of organic dyes by powder and nanotubes TiO₂”, *Ultrasonics Sonochemistry*, v.19, n.3, pp. 642-651, 2012.

[31] FANG, D., LUO, ZH., LIU, S., et al, “Photoluminescence properties and photocatalytic activities of zirconia nanotube arrays fabricated by anodization”, *Optical Materials* , v.35, pp. 1461-1466, 2013.

[32] PRADES, J.D., JIMENEZ-DIAZ, R., HERNANDEZ-RAMIREZ, F. “Toward a Systematic Understanding of Photodetectors Based on Individual Metal Oxide Nanowires”, *Journal of Physical Chemistry C*, v.112 n. 37, pp.14639–14644, 2008.